

# PULSED RF HEATING PARTICULARITIES IN NORMAL-CONDUCTING L-BAND CAVITIES

V. Paramonov, A.K. Skasyrskaya, INR, 117312 Moscow, Russia,  
 K. Floettmann, F. Stephan, DESY, Germany

## Abstract

For present projects, such as X-FEL and ILC, the technology of superconductivity is chosen for the main linacs. However, in some special parts, NC cavities are applied, operating with high electric and magnetic fields. RF gun cavities with an electric field up to  $60 \frac{MV}{m}$  at the photo cathode are now under development. Capture cavities in the ILC positron source should operate with an accelerating gradient of up to  $15 \frac{MV}{m}$ , practically the same value ( $14 \frac{MV}{m}$ ), as for the CDS booster cavity in the Photo Injector Test Facility at DESY in Zeuthen (PITZ). High field strength leads to high specific RF heat loading. In combination with long RF pulses ( $\sim 1ms$ ) it results in substantial surface temperature rise, small cavity shape deformations and measurable frequency shifts. In this report we discuss both particularities and some general regularities related to long pulse operation of L-band cavities. Results of 3D numerical simulations for cavity surface temperature, displacements distributions and corresponding frequency shifts for different cavities are presented and compared with existing experimental data.

## INTRODUCTION

RF pulse heating is a well known problem for very high frequency ( $\geq 3 \cdot 10^9 Hz$ ) high rf power hardware and makes conditional upon wishes for high electric fields. There are a lot of papers, describing this topic study, for example [1] and related references. At L-band frequency maximal electric fields are. Together with lower surface resistance  $R_s = 9.4 \cdot 10^{-3} Ohm$ , it leads to lower values of dissipated rf power density  $P_d = \frac{R_s H^2}{2}$ , as compared, for example with X-band NLC or  $30GHz$  CLIC accelerating structures. Even for some special L-band cavities, operating with significant field values, the pulsed surface rf heating takes place mainly due to long ( $\sim 1ms$ ) RF pulse. The purpose of this paper is to estimate cavities rf parameters change during rf pulse.

## THERMAL ANALYSIS

During rf pulsed heating we have heat propagation from the surface into cavity body with enough sharp temperature front. Two parameters are most important for this effect description - surface temperature rise  $T_s$  at the rf pulse  $\tau$  time and diffusion length  $D_d$  - the distance of temperature decreasing (along the normal direction inside cavity body)

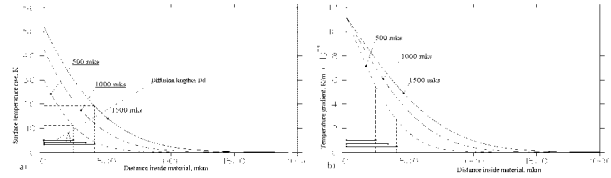


Figure 1: Temperature (a) and temperature gradient (b) distributions near surface for pulse heated OFC tube for different rf pulse length,  $P_d = 4.37 \cdot 10^7 \frac{W}{m^2}$ .

in  $e$  times, see for example, [1]:

$$T_s = \frac{P_d \sqrt{\tau}}{2\sqrt{\pi \rho k c_\epsilon}}, \quad D_d = \sqrt{\frac{k\tau}{\rho c_\epsilon}}, \quad T_s = \frac{P_d D_d}{2\sqrt{\pi k}}, \quad (1)$$

where  $\rho = 8.95 \cdot 10^3 \frac{kg}{m^3}$ ,  $k = 391 \frac{W}{m \cdot K}$  and  $c_\epsilon = 385 \frac{J}{kg \cdot K}$  are the density, the heat conductivity and the specific heat for OFC copper.

Numerically calculated (1D) temperature  $T(r)$  and gradient  $G(r)$  distributions for uniformly pulse heated OFC tube with  $P_d = 4.37 \cdot 10^7 \frac{W}{m^2}$  are shown in Fig. 1. For the pulse length  $\tau = 0.5ms; 1.0ms; 1.5ms$  the  $D_d$  values (1) are  $D_d = 238\mu m; 337\mu m; 413\mu m$  respectively.

To investigate 3D cavities, we improve our previous pro-

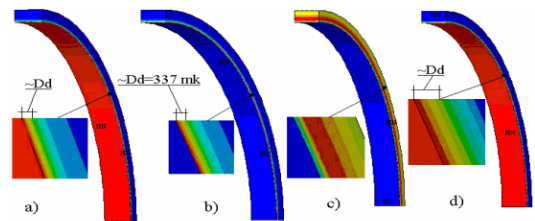


Figure 2: Temperature (a), temperature gradient (b), displacements (c) and stress (d) distributions for pulse heated segment of OFC tube,  $P_d = 4.37 \cdot 10^7 \frac{W}{m^2}$ ,  $\tau = 1ms$ .

cedure of closed-loop 3D cavities analysis [2]. Special meshing technique is developed to ensure precise complete thermal-stress analysis in very thin ( $\sim (1.5 \div 1.8)D_d$ ) 3D layer at the surface of relatively big  $\approx 200mm$  cavity, together with the cavity itself, with ordinary computing resource. Thermal analysis we perform as a direct numerical solution of non-stationary heat transfer equation for the time of rf pulse  $\tau$ . The procedure has been tested at the segment of uniformly pulsed heated tube, where thermal parameters can be precisely calculate with another way, see Fig. 1, and for stress problem there is analytical solution

[3]. Directly calculated temperature, gradient, displacements and stress distributions are shown in Fig. 2. One can see fine foliated structure in distributions. Relative errors for parameters calculations are estimated as  $\sim \pm 0.02\%$  for  $T_s$  with respect (1),  $\sim \pm 15\%$  for displacements (and related cavity frequency shift),  $\sim \pm 20\%$  for maximal stress value.

For DESY 1.5 cell L-band RF Guns (see, for example,[4]),

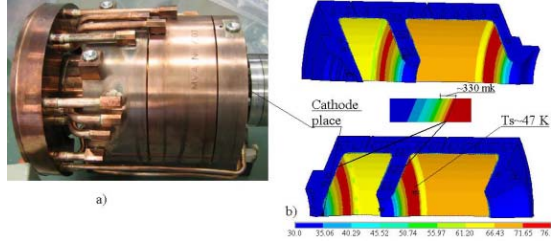


Figure 3: DESY 1.5 cell RF Gun a) and calculated surface temperature rise  $T_s$  distribution at the cavity internal surface after  $\tau = 1ms$ ,  $E_k = 60.0 \frac{MV}{m}$ .

Fig. 3a, operations with electric field at the cathode  $E_c = 60.0 \frac{MV}{m}$  rf input pulse power  $P_{in}$  should be  $P_{in} \approx 6.7MW$ , assuming real quality factor as 0.95 from calculated one. Maximal magnetic field value at the surface, coupled with  $E_c = 60.0 \frac{MV}{m}$ , is  $H_{smax} \approx 10^5 \frac{A}{m}$ , resulting in maximal rf pulse loss density  $P_{dmax} \approx 4.7 \cdot 10^7 \frac{W}{m^2}$ . The calculated  $T_s$  distribution at the cavity surface after  $\tau = 1ms$  rf pulse is shown in Fig. 3b. Maximal  $T_s$  value is  $\approx 46.9K$ . During rf pulse, heat penetrates into the cavity body at the length  $\sim 2D_d \leq 1mm$ . All elements of the cavity design, such as cooling channels, as a rule, are placed at larger distance from the surface. Cavity engineering design is not important for pulsed thermal effect. Heat propagation in tangential directions also negligible, due to small  $P_d$  variations at the distance  $\sim D_d$ . At the cavity surface  $T_s$  distribution repeats very well  $P_d$  one. Heat energy  $W_h$ , stored in the pulse heated layer is  $W_h = P_{in}\tau \approx 6.7kJ$ .

Cavity engineering design is important for total surface temperature rise  $T_{s-tot}$  value, which is a sum of average surface temperature rise  $T_{s-av}$  with pulse related rise  $T_s$ . We specially consider the temperature rise, counting real temperature value at the cavity surface with respect input cooling water temperature  $T_{w-in}$ . For the duty cycle 1% ( $\tau = 1ms$ , Repetition Rate ( $RR$ ) =  $10Hz$ ) operation, average rf power  $P_{av}$ , dissipated in the RF gun cavity, is also significant,  $P_{av} \approx 67kW$ . Cavities have developed cooling circuits, but for high  $P_{av}$  value the maximal  $T_{s-av}$  value is estimated as  $T_{s-av} \approx 35K$  for DESY Gun 4 design and  $T_{s-av} \approx 52K$  for BESSY Gun [5]. The BESSY Gun is constructed for the test program and the presented [5] design is not the final one. Calculated  $T_{s-av}$  distributions are shown in Fig. 4. These  $T_{s-av}$  distribution at the cavity surfaces and corresponding temperature distributions in bodies represent the temperature distributions before rf pulse

beginning. Applying pulse heat load  $P_d$  and calculating heat propagation during rf pulse time, we get surface temperature rise distributions  $T_{s-tot}$ , which are shown in Fig. 4c and Fig. 4d, after rf pulse. Maximal  $T_{s-tot}$  values are  $\approx 79K$  and  $\approx 100K$  for DESY and BESSY cavities, respectively.

Surface temperature increasing leads to  $R_s$  rise and cav-

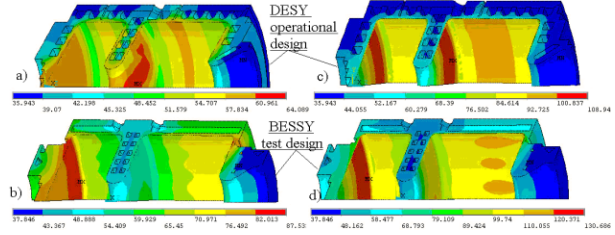


Figure 4: Surface temperature distributions before (a,b) and after (c,d) rf pulse for DESY Gun4 (a,c) and BESSY (b,d) cavities.  $T_{w-in} = 30C^\circ$ ,  $E_c = 60 \frac{MV}{m}$ ,  $\tau = 1000\mu s$ ,  $RR = 10Hz$ .

ity  $Q$ -factor degradation. Calculated  $\frac{\delta Q}{Q} \sim T_s$  decreasing during rf pulse, due to  $T_{s-tot}$  rise, is  $-7.1\%$ . Assuming  $P_{in} = const$ , in mean relative electric field decreasing during rf pulse  $\frac{\delta E}{E} = \frac{\delta Q}{2Q}$ .

PITZ CDS booster cavity [6] cells, Fig. 5a, have es-

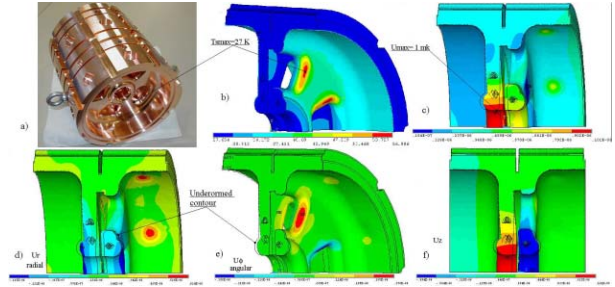


Figure 5: CDS cells (a),  $T_s$  distribution (b), total displacements (c), radial (d), angular (e) and longitudinal (f) components of displacements.  $E_0T = 14 \frac{MV}{m}$ ,  $\tau = 1ms$ .

entially 3D shape with coupling windows and magnetic field concentration at windows ends. Calculated  $T_s$  distribution is shown in Fig. 5b for accelerating gradient  $E_0T = 14 \frac{MV}{m}$ ,  $\tau = 1ms$ , resulting in  $T_{smax} \approx 27K$ .

## PULSED CAVITY DEFORMATIONS

Thin heated layer at the cavity surface expands, both in normal  $\vec{n}$ , and tangential  $\vec{\tau}_d$  directions. The values for corresponding stress  $\sigma_n, \sigma_{\tau_d}$  in this layer one can estimate from general relations [3], assuming 1D normal heat propagation:

$$\sigma_n = \frac{\alpha T E_{el}}{3(1-2\nu)}, \quad \sigma_{\tau_d} = \frac{\alpha T E_{el} \nu}{3(1-2\nu)(1-\nu)}, \quad (2)$$

where  $\alpha = 1.67 \cdot 10^{-5} \frac{1}{K}$ ,  $\nu = 0.345$  and  $E_{el} = 1.23GPa$  are the linear expansion coefficient, Poisson ratio and

Young module for fully annealed OFE copper. For  $T_s \leq 50K$  maximal stress values, all time realized at the surface, are  $\approx 10^6 Pa$ , well below copper yield limit, and cavity deformation is elastic. The final cavity deformation is a result of deforming force, induced in heated layer, interaction with cavity body. It depends on the cavity engineering design and quite different pictures for displacements, shown in Fig. 5, can arise. DESY cavities have a rigid Stainless Steel (SS) jackets in the design. It restricts radial cavity expansion and displacements are mainly longitudinal, Fig. 6a,c. Supposing joint SS jacket, Fig. 6b, we restrict and reduce displacements in both directions. BESSY cavity, Fig. 6d, is constructed from copper totally. For uniform cavity material displacements do not depend on  $E_{el}$  value. The energy  $W_e$ , stored in elastic deformation, is calculated as  $\approx 2.2J$  for all options, shown in Fig. 6

For elastic deformations the displacements values are

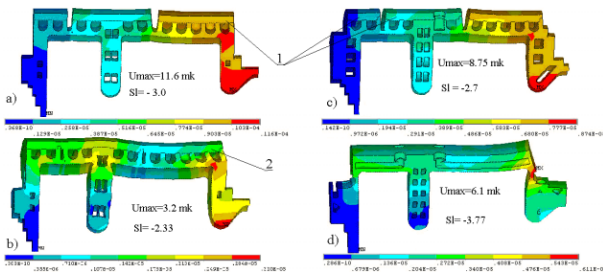


Figure 6: Displacements distributions, induced by pulsed heating, for DESY Gun3 (a,b), Gun 4 (c) and BESSY Gun (d).  $E_c = 60 \frac{MV}{m}$ ,  $\tau = 1ms$ . 1 - segregated SS jackets, 2 - solid SS one.

linearly proportional to the total force value  $F$ . As one can see from (2), both  $\sigma_n$  and  $\sigma_{\tau_d}$  (pressure dimension)  $\sim T$ . Considering expansion, induced by forces in **thin**, no uniformly (in **one** direction) heated surface layer [3], one can find, that **force values**, both  $F_n$ , and  $F_{\tau_{au_d}}$ , are proportional to  $\int T(n)dn$ . This integral is linearly (assuming constant material properties) proportional to the heat amount, deposited in the layer, or  $W_h$  value. The cavity frequency shift  $\delta f$  is linearly proportional to displacements. Instead of complicated  $T_s$  distribution and  $\sim \sqrt{t}$  time dependence, regardless to the cavity engineering design, cavity frequency detuning linearly rises with the time from rf pulse beginning. Parameter  $S_l = \frac{\delta f(\tau)}{P_{in}\tau}$  is the characteristic of the given cavity. This conclusion is in agreement with  $\delta f$  calculations for different  $\tau$  and in agreement with experimental data [7]. Calculated  $S_l$  values, measured in  $\frac{kHz}{MW \cdot ms}$ , are shown in Fig. 6. The  $S_l$  value, extracted from experimental detuning measurements for Gun2 cavity is  $S_l \approx -3.7 \frac{kHz}{MW \cdot ms}$ .

CDS booster will operate with lower  $P_d$  values and displacements distribution after  $\tau = 1ms$  rf pulse are shown in Fig. 5c-f for designed  $E_0 T = 14 \frac{MV}{m}$  value. Calculated displacements are  $\sim 1\mu m$  and calculated detuning is  $\delta f = 4.5kHz$ . Differing from another considered

cavities, including [8], CDS structure has positive  $\delta f$  value. Qualitative analysis of displacements components (see Fig. 5d-f) allows us explain this cavity particularity. cavity deformation, induced by expansion of hot spot at the window ends, results in drift tubes displacement.

RF Guns operation with  $E_c = 60 \frac{MV}{m}$  is an advanced

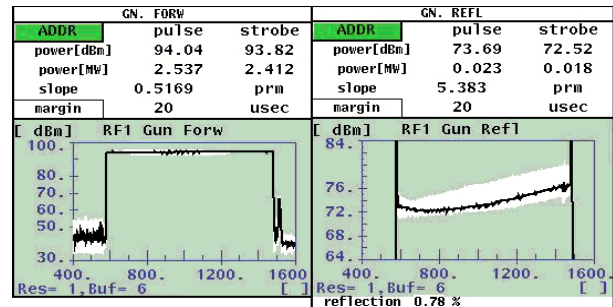


Figure 7: Time diagram for incident (left) and reflected (right) rf power during rf pulse  $\tau = 1ms$  for normal RF gun operation.

regime. The normal one corresponds to  $E_c = 40 \frac{MV}{m}$ , resulting in 0.44 scaling for rf power,  $T_s$  and another related parameters values. From rf reflected power time diagram for normal RF Gun operation, Fig. 7b, one can see reflection coefficient change. It means cavity own frequency and quality factor change during rf pulse. But main effect of the cavity detuning may be in variable phase shift between cavity field and rf source one.

## SUMMARY

L-band NC cavities, designed for special regimes operations, will have measurable rf parameters change due to pulsed heating during long rf pulse. The presented results are the input for cavities operation analysis, further optimization and sub-systems improvements.

## REFERENCES

- [1] D. Pritzkau. RF Pulsed Heating. SLAC-R-577, 2001.
- [2] S.C. Joshi et al., The complete 3D coupled RF-thermal-structural-RF analysis ... LINAC02, p. 216, 2002.
- [3] L. Landau, E. Lifshitz. Theoretical physics. Theory of elasticity. Nauka, Moscow, 1987, (in Russian).
- [4] A.Oppelt et al., Status and first results from the upgraded PITZ facility. FEL05 Conference, USA, p. 564, 2005.
- [5] F. Marhauser. High power test of a high duty cycle RF photoinjector gun for the BESSY FEL. EPAC2006, p.68, 2006
- [6] V. Paramonov et al., The PITZ Booster Cavity - A Prototype for the ILC PS Cavities. PAC 2005, p. 1030, 2005.
- [7] D. Kotthaus. Design of the Control for the RF Gun of the VUV-FEL Linac. Diplomarbeit. Univ. of Hamburg, 2004.
- [8] J.W. Wang, et al., Studies of Room Temperature Structures for the ILC Positron Source. PAC 2005, p. 2827, 2005.